

# Baryon Stopping as a new Probe of Geometric Scaling

Yacine Mehtar-Tani and Georg Wolschin

*Institut für Theoretische Physik der Universität Heidelberg,  
Philosophenweg 16, D-69120 Heidelberg, Germany*

(Dated: February 26, 2019)

We suggest to use net-proton rapidity distributions in central relativistic heavy-ion collisions at SPS, RHIC and LHC energies in order to probe saturation physics. Within the color glass condensate framework based on small-coupling QCD, net-baryon rapidity distributions are shown to exhibit geometric scaling. Excellent agreement with RHIC data in Au + Au collisions at  $\sqrt{s_{NN}} = 62.4$  GeV and 200 GeV is found, in particular in the fragmentation regions. Predictions for net-proton rapidity spectra and the mean rapidity loss in central Pb + Pb collisions at LHC energies of  $\sqrt{s_{NN}} = 5.52$  TeV are made.

PACS numbers: 24.85.+p, 25.75.-q, 25.75.Dw, 12.38.Mh

Baryon stopping in relativistic heavy-ion collisions as a probe of QCD-matter at high parton density is of great current interest [1, 2, 3, 4]. Theoretical QCD-based approaches usually focus on charged-hadron production. In the central rapidity region a reasonable understanding has been achieved in the color glass condensate (CGC) framework [5, 6, 7, 8] through inclusive gluon production [9, 10]. In this theory, due to the self-interaction of gluons, the number of gluons in the nuclear wave function increases with increasing energy and decreasing longitudinal momentum fraction  $x$  carried by the parton.

Unitarity requires that the gluon density saturates below a characteristic momentum scale, the so-called saturation scale  $Q_s$ . In this regime gluons form a coherent state. Presently the evidence for the existence of this state of matter is, however, not yet clear. Due to the dependence of the saturation scale on rapidity and mass number, it has been proposed that saturation effects should be studied with heavy nuclei and large rapidities at RHIC energies and beyond.

In this Letter we suggest to use the rapidity distribution of net protons ( $p - \bar{p}$ ) in central heavy-ion collisions as a testing ground for saturation physics, cf. Fig. 1. In  $A + A$  collisions, two distinct and symmetric peaks with respect to rapidity  $y$  occur at SPS energies [11] and beyond. The rapidity separation between the peaks increases with energy, and decreases with increasing mass number  $A$  reflecting larger baryon stopping for heavier nuclei, as has been investigated phenomenologically in the relativistic diffusion model [12].

The net-baryon number is essentially transported by valence quarks. During the collision the fast valence quarks in one nucleus scatter in the other nucleus by exchanging soft gluons, leading to their redistribution in rapidity space. Here we do not address the issue of the baryon transport mechanism in the fragmentation process [13] that is relevant for identified baryons.

We take advantage of the fact that the valence quark parton distribution is well known at large  $x$ , which corresponds to the forward and backward rapidity region, to access the gluon distribution at small  $x$  in the target nucleus. Therefore, this picture provides a clean probe

of the unintegrated gluon distribution  $\varphi(x, p_T)$  at small  $x$  in the saturation regime. Here  $p_T$  is the transverse momentum transfer.

We have two symmetric contributions, coming from the two beams. The contribution of the fragmentation of the valence quarks in the forward moving nucleus is given by the simple formula [14] for the rapidity distribution of hadrons:

$$\frac{dN}{dy} = \frac{C}{(2\pi)^2} \int \frac{d^2 p_T}{p_T^2} x_1 q_v(x_1, Q_f) \varphi(x_2, p_T), \quad (1)$$

where  $x_1 = p_T/\sqrt{s} \exp(y)$ ,  $x_2 = p_T/\sqrt{s} \exp(-y)$  are the longitudinal momentum fractions carried, respectively, by the valence quark in the projectile and the soft gluon in the target. The factorization scale is set equal to the transverse momentum,  $Q_f \equiv p_T$ . The contribution of valence quarks in the other beam nucleus is added incoherently by changing  $y \rightarrow -y$ . The gluon distribution is related to the forward dipole scattering amplitude  $\mathcal{N}(x, r_T)$ , for a quark dipole of transverse size  $r_T$ , through the Fourier transform

$$\varphi(x, p_T) = 2\pi p_T^2 \int r_T dr_T \mathcal{N}(x, r_T) J_0(r_T p_T). \quad (2)$$

In the fragmentation region of the projectile the valence quark parton distribution function (PDF) is dominated by large values of  $x_1$ . We integrate out the fragmentation function such that the hadron rapidity distribution is proportional to the parton distribution. The overall constant  $C$  depends on the nature of the produced hadron.

One important prediction of the color glass condensate theory is geometric scaling: the gluon distribution depends on  $x$  and  $p_T$  only through the scaling variable  $p_T^2/Q_s^2(x)$ , where  $Q_s^2(x) = A^{1/3} Q_0^2 x^{-\lambda}$ ,  $A$  is the mass number and  $Q_0$  sets the dimension. This has been confirmed experimentally at HERA [15]. The fit value  $\lambda = 0.2 - 0.3$  agrees with theoretical estimates based on next-to-leading order Balitskii-Fadin-Kuraev-Lipatov (BFKL) results [16, 17]. To show that the net-baryon distribution reflects the geometric scaling of the gluon dis-

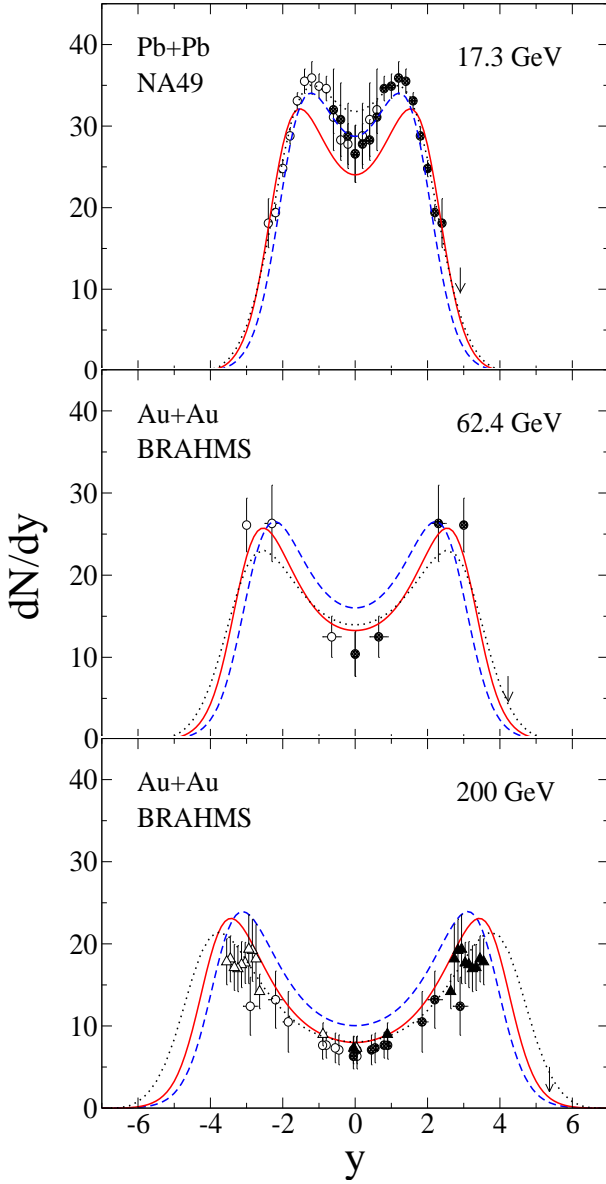


FIG. 1: (color online). Rapidity distribution of net protons in central (0 - 5%) Pb + Pb collisions at SPS energies of  $\sqrt{s_{NN}} = 17.3$  GeV (top frame). The theoretical results are compared with NA49 data [11]. Solid curves are for  $Q_0^2 = 0.034$  GeV<sup>2</sup> and  $\lambda = 0.288$ , dashed curves are for  $Q_0^2 = 0.068$  GeV<sup>2</sup>, producing more stopping. The dotted curves are for  $Q_0^2 = 1.2$  GeV<sup>2</sup> and  $\lambda = 0$ . At RHIC energies of  $\sqrt{s_{NN}} = 62.4$  GeV (middle frame, 0 - 10%) and 200 GeV (bottom frame, 0 - 5%) for central Au + Au, our corresponding theoretical results are compared with BRAHMS net proton data [1, 2]. At 200 GeV, triangles are preliminary BRAHMS data points for 0 - 10% [18]. Arrows indicate the beam rapidities.

tribution, we perform the following change of variables:

$$x \equiv x_1, \quad x_2 \equiv x e^{-2y}, \quad p_T^2 \equiv x^2 s e^{-2y}. \quad (3)$$

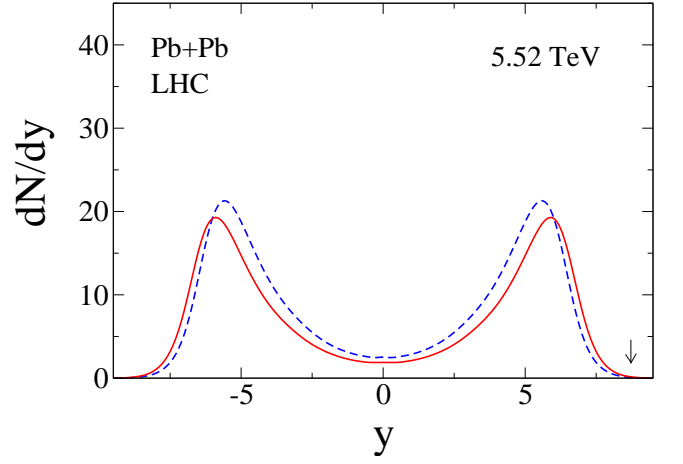


FIG. 2: (color online). Rapidity distribution of net protons in central Pb + Pb collisions at LHC energies of  $\sqrt{s_{NN}} = 5.52$  TeV. The theoretical distribution for the fragmentation sources is shown for two values of the saturation scale as in Fig. 1.

Thus, we rewrite Eq. (1) as

$$\frac{dN}{dy}(\tau) = \frac{C}{2\pi} \int_0^1 \frac{dx}{x} x q_v(x) \varphi(x^{2+\lambda} e^\tau), \quad (4)$$

where  $\tau = \ln(s/Q_0^2) - \ln A^{1/3} - 2(1 + \lambda)y$  is the corresponding scaling variable. Hence, the net-baryon multiplicity in the peak region is only a function of a single scaling variable  $\tau$ , which relates the energy dependence to the rapidity and mass number dependence. In the fragmentation region, the valence quark distribution is only very weakly dependent on  $Q_f$ .

From the equation for the isolines,  $\tau = \text{const}$ , one gets the evolution of the position of the fragmentation peak in the forward region with respect to the variables of the problem

$$y_{\text{peak}} = \frac{1}{1 + \lambda} \left( y_{\text{beam}} - \ln A^{1/6} \right) + \text{const}, \quad (5)$$

where  $y_{\text{beam}} = 1/2 \cdot \ln[(E + p_L)/(E - p_L)] \simeq \ln \sqrt{s}/m_0$  is the beam rapidity at beam energy  $E$  and longitudinal momentum  $p_L$  with the nucleon mass  $m_0$ .

To take into account saturation effects in the target we choose the Golec-Biernat-Wüsthoff model [19] for the forward dipole scattering amplitude  $\mathcal{N}$ , leading to (cf. Eq. (2) and [14])

$$\varphi(x, p_T) = 4\pi \frac{p_T^2}{Q_s^2(x)} \exp\left(-\frac{p_T^2}{Q_s^2(x)}\right). \quad (6)$$

The valence quark parton distribution of the nucleus is taken to be equal to the valence quark PDF in a nucleon times the number of participants in the nucleus. We are focusing here on the forward rapidity region, and interpolate to mid-rapidity where small- $x$  quarks are dominant, by matching the leading-order distributions [20] and the Regge trajectory,  $xq_v \propto x^{0.5}$ , at  $x = 0.01$  [3].

Our results for net-proton rapidity distributions in central Pb + Pb and Au + Au collisions are shown in Fig. 1. Solid curves are for  $Q_0^2 = 0.034 \text{ GeV}^2$  and  $\lambda = 0.288$  [19]. Dashed curves are for twice the value of  $Q_0^2$  producing slightly more stopping, as would also be the case for a larger value of  $A$ . These two values correspond to  $Q_s^2 = 0.77 \text{ GeV}^2$  and  $1.54 \text{ GeV}^2$  at  $x = 0.01$ , respectively. We compare with SPS NA49 Pb + Pb data at  $\sqrt{s_{NN}} = 17.3 \text{ GeV}$  [11], and BRAHMS Au + Au data at 62.4 GeV and 200 GeV [1, 2]. Our prediction for central Pb + Pb at 5.52 TeV LHC energies is shown in Fig. 2, again for the above two values of the saturation scale. At LHC energies the mid-rapidity region is almost charge (baryon) free, and we obtain  $dN/dy(y=0) \simeq 1-3$  for net protons.

We have normalized the total yield to the number of proton participants,  $N_p \simeq 140$  for both, central Au + Au and Pb + Pb. Note that whereas baryon number is conserved, this is not necessarily the case for the number of net protons. Hence, the integral of the experimental distribution may be smaller than the number of participants. Our results regarding geometric scaling are, however, independent of the integrated yield since we are mainly focussing on the position of the fragmentation peaks.

Physically, the two peaks represent the result of the scattering of the fast moving projectile valence quarks in the target, they are deflected, their distribution broadens and carries information about the gluon distribution in the target. This is in analogy to x-rays that are deflected by a crystal and carry information about its structure.

With increasing energy the peaks move apart, the solutions behave like travelling waves in rapidity space [21], which can be probed experimentally at distinct values of the beam energy, or the corresponding beam rapidity. We have derived the peak position as a function of the beam rapidity as  $y_{\text{peak}} = v y_{\text{beam}} + \text{const}$  with the peak velocity  $v = 1/(1 + \lambda)$ , cf. Eq. (5). The position of the peak in rapidity space as a function of the beam energy can in principle be determined experimentally, or at least estimated (RHIC). Theoretically, its evolution with energy provides a measure of the saturation scale exponent  $\lambda$ . Hence, a precise determination of the net-proton fragmentation peak position as a function of beam energy would provide detailed information about the gluon saturation scale.

In Fig. 3, we have plotted our numerical result for the peak position as a function of  $y_{\text{beam}}$ . It grows linearly with beam rapidity, the slope is  $v = 0.776$  for  $\lambda = 0.288$ . The mean rapidity loss  $\langle \delta y \rangle = y_{\text{beam}} - \langle y \rangle$  is also calculated, and our result is in agreement with the experimental values of baryon stopping that have been obtained at AGS and SPS energies [11, 22], and at the lower RHIC energy of 62.4 GeV.

At the higher RHIC energy of 200 GeV, however, our model predicts a larger mean rapidity loss than what has been estimated from the BRAHMS data [1]. This discrepancy could be related to the extrapolation proce-

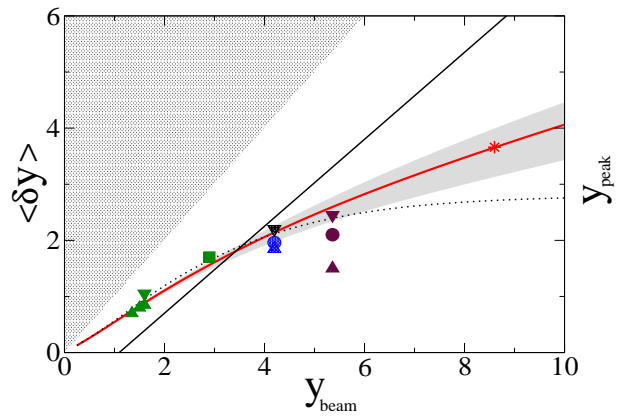


FIG. 3: (color online). The mean rapidity loss  $\langle \delta y \rangle$  as obtained from our theoretical results is plotted as a function of beam rapidity  $y_{\text{beam}}$ , solid curve. The star at  $y_{\text{beam}} = 8.68$  is our prediction for central Pb + Pb at LHC-energies of  $\sqrt{s_{NN}} = 5.52 \text{ TeV}$  with  $Q_0^2 = 0.034 \text{ GeV}^2$  and  $\lambda = 0.288$  (the band is for varying  $\lambda = 0.2 - 0.35$ ), the dotted curve is for  $\lambda = 0$  (no x-dependence), and  $Q_0^2 = 1.2 \text{ GeV}^2$ . The solid straight line shows our prediction for the position of the fragmentation peaks,  $|y_{\text{peak}}|$ . Analysis results from AGS Au + Au data (E917, E802/E866, triangles) [22], SPS Pb + Pb data (NA49, square) [11], RHIC Au + Au data (BRAHMS, dots, with triangles as lower and upper limits) [1, 2] are also shown.

dure done by the BRAHMS collaboration towards non-measured rapidities  $|y| > 3.2$  where the peaks stand.

It is also conceivable that up to the highest RHIC energies the scaling regime with  $\lambda \simeq 0.3$  is not yet fully reached. Indeed our calculation with  $\lambda = 0$  and a value of  $Q_0^2 = 1.2 \text{ GeV}^2$  that we have adjusted to the fragmentation peak position at SPS energy (Fig. 1) gives better agreement with the low-energy data, as shown by the dotted curve in Fig. 3. This emphasizes the importance of a detailed measurement at LHC energies to allow more definite conclusions about the value of  $\lambda$ , which would then be determined by the slope of the mean rapidity loss at high beam rapidity above RHIC (solid curve in Fig. 3).

Assuming that the mean rapidity evolves similarly to the peak position,  $\langle y \rangle \equiv y_{\text{peak}} + \text{const.}$ , the linear increase of the mean rapidity loss at large energies corresponding to beam rapidities  $y_{\text{beam}} > 5$  is given by

$$\langle \delta y \rangle = \frac{\lambda}{1 + \lambda} y_{\text{beam}} + \text{const.} \quad (7)$$

Hence, the mean rapidity loss that accompanies the energy loss in the course of the slow-down of baryons provides at large beam rapidities  $y_{\text{beam}} > 5$  a measure for  $\lambda$  and thus, a test of saturation physics. The case  $\lambda = 0$ , or equivalently  $Q_s$  constant, leads to a saturation of the mean rapidity loss at high energies, and correspondingly at large beam rapidities.

In the peak region, the average  $x$  in the projectile is  $x \simeq 0.2 - 0.3$ , which corresponds to the average momen-

tum fraction carried by a valence quark. In the target,  $x = (0.2 - 0.3)e^{-2y_{\text{peak}}}$ , it decreases with increasing energy. In this kinematic regime we have a natural intrinsic hard momentum, the saturation scale  $Q_s$ . This justifies the use of small-coupling techniques in QCD for calculating integrated yields [23]. The effects of the medium are expected to be small at forward rapidity since the fast moving valence quarks escape the interaction zone quickly. A detailed measurement of the peak region would then enable us to reconstruct the gluon distribution from Eq. (1).

To summarize, we have presented a saturation model for net-baryon distributions that successfully describes net-proton rapidity distributions and their energy and mass dependence. The remarkable feature of geometric scaling predicted by the CGC is reflected in the net-baryon rapidity distribution, providing a direct test of

saturation physics.

In particular, we have shown that the peak position in net-proton rapidity distributions of centrally colliding heavy ions at ultra-relativistic energies obeys a scaling law involving the mass number and the beam energy. Our result for the mean rapidity loss in  $\sqrt{s_{NN}} = 200$  GeV Au + Au is significantly larger than the BRAHMS result, which, however, contains an extrapolation to the unmeasured region. This emphasizes the importance of a detailed analysis at LHC energies.

One of the authors (Y. M.-T.) acknowledges critical comments by Jamal Jalilian-Marian and Mark Strikman. We are grateful to the BRAHMS collaboration for their preliminary data. This work has been supported by the Deutsche Forschungsgemeinschaft under Grant No. STA 509/1-1.

- 
- [1] I.G. Bearden *et al.* (BRAHMS Collaboration), Phys. Rev. Lett. **93**, 102301 (2004).
  - [2] H.H. Dalsgaard *et al.* (BRAHMS Collaboration), Int. J. Mod. Phys. E **16**, 1813 (2007); I.C. Arsene *et al.* (BRAHMS Collaboration), arXiv:0901.0872 (2009), submitted to Phys. Lett. B.
  - [3] K. Itakura, Y.V. Kovchegov, L.D. McLerran, and D. Teaney, Nucl. Phys. **B730**, 160 (2004).
  - [4] J.L. Albacete, Y.V. Kovchegov, and K. Tuchin, Nucl. Phys. **A781**, 122 (2007).
  - [5] L.V. Gribov, E.M. Levin, and M.G. Ryskin, Phys. Rep. **100**, 1 (1983); A.H. Mueller and J. Qiu, Nucl. Phys. **B268**, 427 (1986); J.P. Blaizot and A.H. Mueller, Nucl. Phys. **B289**, 847 (1987); L. McLerran and R. Venugopalan, Phys. Rev. D **49**, 2233 (1994).
  - [6] I. Balitsky, Nucl. Phys. **B463**, 99 (1996); Y.V. Kovchegov, Phys. Rev. D **60**, 034008 (1999).
  - [7] J. Jalilian-Marian, A. Kovner, A. Leonidov, and H. Weigert, Nucl. Phys. **B504**, 415 (1997); J. Jalilian-Marian, A. Kovner, and H. Weigert, Phys. Rev. D **59**, 014015 (1998); J. Jalilian-Marian, A. Kovner, A. Leonidov, and H. Weigert, Phys. Rev. D **59**, 034007 (1999); Erratum, 099903 (1999).
  - [8] E. Iancu, A. Leonidov, and L.D. McLerran, Nucl. Phys. **A692**, 583 (2001); Phys. Lett. B **510**, 133 (2001).
  - [9] D. Kharzeev, E. Levin, and M. Nardi, Nucl. Phys. **A730**, 448 (2004); Nucl. Phys. **A747**, 609 (2005).
  - [10] J.L. Albacete, Phys. Rev. Lett. **99**, 262301 (2007).
  - [11] H. Appelshäuser *et al.* (NA49 Collaboration), Phys. Rev. Lett. **82**, 2471 (1999).
  - [12] G. Wolschin, Eur. Phys. J. A **5**, 85 (1999); Europhys. Lett. **47**, 30 (1999); **74**, 29 (2006); Phys. Rev. C **69**, 024906 (2004); Prog. Part. Nucl. Phys. **59**, 374 (2007).
  - [13] G.C. Rossi and G. Veneziano, Phys. Rep. **63**, 153 (1980); D. Kharzeev, Phys. Lett. B **378**, 238 (1996); S.E. Vance, M. Gyulassy, and X.N. Wang, Phys. Lett. B **443**, 45 (1998).
  - [14] D. Kharzeev, Y.V. Kovchegov, and K. Tuchin, Phys. Lett. B **599**, 23 (2004); R. Baier, Y. Mehtar-Tani, and D. Schiff, Nucl. Phys. **A764**, 515 (2006); A. Dumitru, A. Hayashigaki, and J. Jalilian-Marian, Nucl. Phys. **A765**, 464 (2006).
  - [15] A. M. Staśto, K. Golec-Biernat, and J. Kwieciński, Phys. Rev. Lett. **86**, 596 (2001).
  - [16] L.N. Lipatov, Sov. J. Nucl. Phys. **23**, 338 (1976); E. A. Kuraev, L.N. Lipatov, and V.S. Fadin, Sov. Phys. JETP **45**, 199 (1977); I.I. Balitskii and L.N. Lipatov, Sov. J. Nucl. Phys. **28**, 822 (1978).
  - [17] D.N. Triantafyllopoulos, Nucl. Phys. **B648**, 293 (2003).
  - [18] R. Debbe *et al.* (BRAHMS Collaboration), J. Phys. G **35**, 104004 (2008).
  - [19] K. Golec-Biernat and M. Wüsthoff, Phys. Rev. D **59**, 014017 (1998).
  - [20] A.D. Martin, R.G. Roberts, W.J. Stirling, and R.S. Thorne, Phys. Lett. B **531**, 216 (2002).
  - [21] S. Munier and R. Peschanski, Phys. Rev. Lett. **91**, 232001 (2003); Phys. Rev. D **69**, 034008 (2004).
  - [22] F. Videbaek and O. Hansen, Phys. Rev. C **52**, 2684 (1995); L. Ahle *et al.* (E802 Collaboration/Experiment E-866), Phys. Rev. C **60**, (1999) 064901. B.B. Back *et al.* (E917 Collaboration), Phys. Rev. Lett. **86**, 1970 (2001).
  - [23] A. Dumitru, L. Gerland, and M. Strikman, Phys. Rev. Lett. **90**, 092301 (2003).